Geophysical Research Letters

RESEARCH LETTER
10.1029/2018GL077879

Key Points:
- We reproduce the timing and amplitude of spontaneous and triggered slow slip events (SSEs) in New Zealand using rate-and-state fault models
- SSE propensity to dynamic triggering mainly depends on the timing of perturbation with respect to the SSE cycle and the maximum Coulomb stress change
- Shallow SSEs are more likely to be dynamically triggered than deep SSEs because of enhanced stress perturbation (magnitude and duration) from the sedimentary wedge

Supporting Information:
- Supporting Information S1

Correspondence to:
M. Wei,
matt-wei@uri.edu

Citation:
Wei, M., Kaneko, Y., Shi, P., & Liu, Y. (2018). Numerical modeling of dynamically triggered shallow slow slip events in New Zealand by the 2016 M_w 7.8 Kaikoura earthquake. *Geophysical Research Letters*, *45*. https://doi.org/10.1029/2018GL077879

Received 9 MAR 2018
Accepted 8 MAY 2018
Accepted article online 16 MAY 2018

Numerical Modeling of Dynamically Triggered Shallow Slow Slip Events in New Zealand by the 2016 M_w 7.8 Kaikoura Earthquake

Meng Wei[1], Yoshihiro Kaneko[2], Pengcheng Shi[1], and Yajing Liu[3]

[1]Graduate School of Oceanography, University of Rhode Island, Narragansett, RI, USA, [2]Department of Earth and Planetary Sciences, GNS Science, Lower Hutt, New Zealand, [3]McGill University, Montreal, Quebec, Canada

Abstract The 2016 M_w 7.8 Kaikoura earthquake triggered widespread slow slip events (SSEs) in the northern Hikurangi subduction zone, providing a unique opportunity to study the mechanism of dynamic triggering of SSEs. Here we simulate SSEs near Gisborne, New Zealand, in the framework of rate-and-state friction. Low effective normal stress (~0.4 MPa) on the shallow subduction interface is needed to reproduce the observed repeating, spontaneous SSEs. Dynamic stress perturbations from the Kaikoura mainshock are adequate to trigger SSEs with characteristics similar to observation. SSE propensity to dynamic triggering mainly depends on the timing of perturbation with respect to the SSE cycle and the maximum Coulomb stress change. Once the perturbation amplitude exceeds an initial threshold, prolonged stress perturbations tend to decrease the triggering threshold hence promote dynamic triggering of SSEs. Therefore, shallow SSEs are more likely to be dynamically triggered than their deep counterparts because of enhanced stress perturbation (magnitude and duration) from the sedimentary wedge.

Plain Language Summary Slow slip events, gradual fault movement lasting days to months, have been documented in subduction zones worldwide. Occasionally, distant earthquakes can trigger these events, but how the triggering happens is still not well understood. Recently, widespread slow slip events have been recorded in the northern Hikurangi subduction zone and are believed to be triggered by the 2016 Kaikoura earthquake in New Zealand. In this study, we develop a computer model for regular, repeating slow slip events in northern Hikurangi and analyze if applying the Kaikoura earthquake waves to the model leads to the triggering of slow slip events. We find that our model can reproduce the observed slow slip events in northern Hikurangi following the Kaikoura earthquake. Our model explains a potential underlying mechanism for the triggering process of slow slip events. Our results further provide insights into how, where, and when slow slip events in subduction zones are triggered by earthquake waves in general.

1. Introduction

Slow slip events (SSEs) in subduction zones have been reported around the world for more than 15 years (Dragert et al., 2001; Peng & Gomberg, 2010; Rogers & Dragert, 2003; Saffer & Wallace, 2015; Schwartz & Rokosky, 2007). They are sometimes accompanied by nonvolcanic tremors and/or low-frequency earthquakes (LFEs), and together, represent an important way of strain release at depths transitioning from seismogenic to stable sliding on the subduction interface (Shelly et al., 2006). Most of the episodic SSEs and nonvolcanic tremors/LFEs in global subduction zones occur spontaneously under hypothesized near-lithostatic fluid pressure conditions (Audet et al., 2009; Liu & Rice, 2007; Peng & Gomberg, 2010). Although distant mainshocks have frequently triggered tremors and LFEs (Miyazawa & Brodsky, 2008; Rubinstein et al., 2007), dynamic triggering of SSEs is rare, with only a few reports with estimated triggering stress amplitudes ranging from 0.6 to 600 kPa and depths ranging from 4 to 40 km (Araki et al., 2017; Itaba & Ando, 2011; Wallace et al., 2017; Zigone et al., 2012). The mechanism of dynamic triggering of SSEs and the reason for relatively rare occurrences are still unclear. Among these reported cases, the well-recorded shallow SSEs along the Hikurangi margin triggered by the 2016 M_w 7.8 Kaikoura (New Zealand) earthquake provide a unique opportunity to study the mechanism of dynamic triggering of SSEs.

SSEs are segmented along the Hikurangi subduction zone in New Zealand (Figure 1a; Wallace & Beavan, 2010; Wallace et al., 2012; Wallace & Eberhart-Phillips, 2013; Wallace et al., 2016). SSEs in the northern (Gisborne)

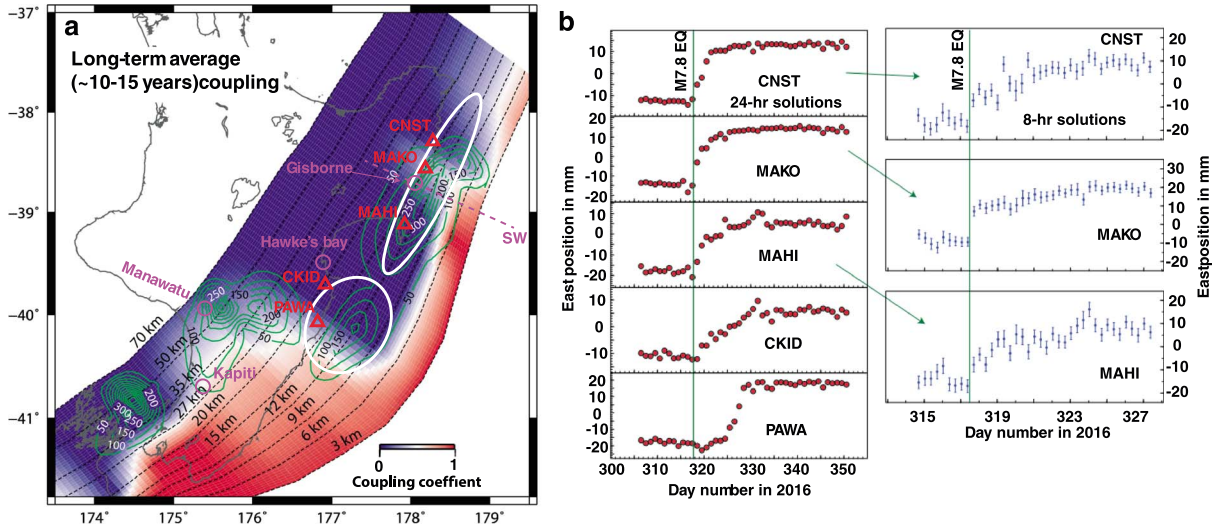

Figure 1. (a) Coupling coefficient on the subduction interface inferred from long-term velocities including SSEs (modified from figures in Wallace & Beavan, 2010, and Wallace et al., 2017). The green contours show total slip (in mm) detected in SSEs between 2002 and 2010. The dashed black lines show depth contours (labeled) to the subduction interface. The white ellipses are the slip area of SSEs triggered by the 2016 M_w 7.8 Kaikoura earthquake. The red triangles are selected GPS stations. The magenta circles are locations for referencing. The dashed magenta line highlights the along-dip profile that we focus on in the simulation (as shown in Figure 2a). (b) East components of continuous GPS time series at stations on the east coast, showing slow slip following the Kaikoura earthquake (modified from Wallace et al., 2017). The vertical green lines show the time of the mainshock. The time series on the left (in red) are positions for each 24-hr period, available at www.geonet.org.nz. Note the onset of SSE slip at cGPS sites further south (PAWA) a few days after the earthquake. The time series on the right (in blue) shows positions for each 8-hr period at a subset of sites at the northern Hikurangi margin north, where SSE displacement initiated immediately.

and middle (Hawke's Bay) segments occur at depths above 15 km, whereas those in the southern segment (Manawatu and Kapiti) occur at depth between 25 and 60 km. Global Positioning System (GPS) records following the 2016 M_w 7.8 Kaikoura earthquake suggest that an SSE was instantaneously triggered in the northern segment with a clear slip step during the first few hours and slow slip that lasted about a week (stations CNST, MAKO, and MAHI in Figure 1b). Slow slip in the middle segment became visible on GPS time series a few days after the mainshock (stations CKID and PAWA in Figure 1b). Wallace et al. (2017) suggested that SSEs on both the northern and middle segments were triggered dynamically because at such distances the static stress change caused by the mainshock is ~1,000 times smaller than the dynamic stress change. Slow slip on the southern segment closer to the mainshock rupture area was also triggered, but the mechanism is complicated because of the similar levels of static and dynamic stress changes as well as the proximity to the afterslip zone (Wallace et al., 2018).

Here we run numerical simulations in the framework of rate-and-state (RS) friction to study the mechanism of dynamic triggering of SSEs of the Hikurangi subduction zone near Gisborne, New Zealand. Variants of RS friction models have been widely applied to simulate the spontaneous slow-slip processes (Hawthorne & Rubin, 2013a, 2013b; D. Li & Liu, 2016, 2017; H. Li et al., 2018; Liu & Rice, 2007; Liu & Rubin, 2010; Luo, 2018; Luo & Ampuero, 2017; Matsuzawa et al., 2013; Rubin, 2008; Segall et al., 2010; Shibazaki et al., 2012; Watkins et al., 2015), statically and dynamically triggered earthquakes (Gomberg et al., 1998; Kaneko & Lapusta, 2008; Perfettini et al., 2003a, 2003b), and dynamically triggered creep events on crustal faults (Wei et al., 2013, 2015). However, the RS friction model has yet not been applied to study the dynamic triggering of SSEs. We build a 2-D continuum model with a 1-D fault, governed by the "standard" RS friction law, following Liu and Rice (2007). Among the variants of RS friction models (discussed in H. Li et al., 2018), our model involves the basics of RS friction and probably the minimum set of assumptions. Next, we develop a reference model using grid search for the optimal set of friction parameters that best reproduce the observations of spontaneous SSEs near the Gisborne segment. We then systematically examine the triggering behavior under realistic stress perturbations of various amplitudes and timing in a SSE cycle.

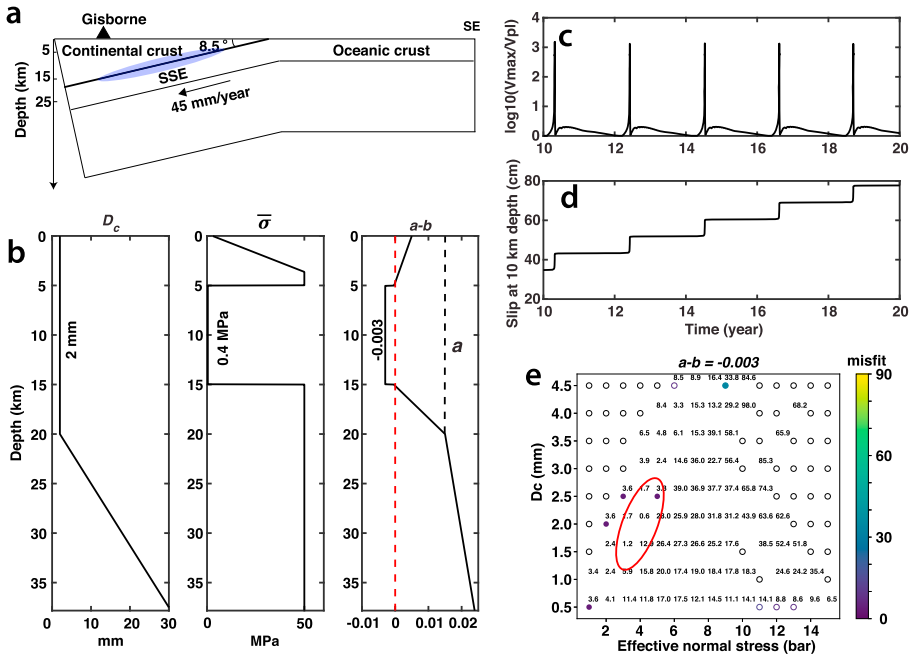

Figure 2. (a) Model setup. The purple shaded area highlights the SSE region. (b) Depth profiles of key parameters of the best fitting model in the rate-and-state simulation. Note that the black dashed line in the *a-b* panel shows the value of *a*. (c) Maximum velocity on the fault. (d) Cumulative slip at 10 km depth. (e) Phase diagram illustrating the dependence of the SSE behavior on friction parameters with $a\text{-}b = -0.003$. The red ellipse highlights the minimum misfit. Note that a full range of input parameters is not explored in this study. However, the SSE behavior can be summarized by the ratio of the nucleation size and the width of the VW zone, as shown in Wei et al. (2013).

2. Reference Model

We simulate SSEs on a 1-D planar thrust fault embedded in a 2-D elastic half-space in the framework of RS friction (quasi-dynamic) with the "aging" evolution law (see the supporting information for details; following Liu & Rice, 2007). We use a planar fault with a dip angle of 8.5° (Figure 2a), which is the average dip angle above 15 km near Gisborne, New Zealand (Williams et al., 2013). The depth distribution of the friction parameter *a-b*, the effective normal stress $\overline{\sigma}$, and the critical slip distance D_c is shown in Figure 2b. Although the profile of *a-b* is similar to the synoptic distribution of a velocity-weakening (VW, $a\text{-}b < 0$) layer encompassed by velocity-strengthening (VS, defined where $a\text{-}b > 0$) layers on the top and bottom, we design the model parameters such that the nucleation size of slip events is comparable to the width of the VW layer (Liu & Rice, 2007; Wei et al., 2015) and such that the VW layer generates SSEs (i.e., slip rate < 1 cm/s) but not earthquakes. The increase of D_c with depth below 20 km is motivated by computational efficiency (Lapusta et al., 2000) and produces the same results for shallow SSEs as using a constant D_c for all depth. The fault is loaded from the bottom at the plate convergence rate at 45 mm/year (Wallace et al., 2004). Shear modulus is set to be 15 GPa (Eberhart-Phillips & Bannister, 2015) to account for the shallow SSE depths.

The value of key parameters *a-b*, $\overline{\sigma}$, and D_c for a reference model are determined using a grid search approach to reproduce the averaged observations of recurrence interval, duration, and maximum cumulative slip of repeating SSEs. A range of simulations is tested with different *a-b* and $\overline{\sigma}$ between 5 and 15 km and D_c above 20 km (Figure 2b). The occurrence of SSEs is defined when the maximum velocity exceeds $3V_{pl}$. The misfit is defined as $\chi = \sqrt{\left(\frac{I_o - I_s}{S(I_o)}\right)^2 + \left(\frac{D_o - D_s}{S(D_o)}\right)^2 + \left(\frac{A_o - A_s}{S(A_o)}\right)^2}$, where I_o, D_o, and A_o are the average interval, duration, and maximum slip of observed SSEs near Gisborne; I_s, D_s, and A_s are those of the modeled spontaneous SSEs; and S is the standard deviation of each observed property (Table S1 in the supporting information). I_o, D_o, and A_o between 2002 and 2015 are 2.0 ± 0.5 year, 15 ± 6 days, and 126 ± 87 mm, respectively (Table S1). The SSE in 2016 is excluded because it was likely triggered by the Kaikoura earthquake and not in its regular cycle. For the modeled SSEs, only events after

the first few SSE cycles are counted to minimize the effect of initial conditions. The parameters of the best fitting model (i.e., minimum misfit) are a-b = −0.003, D_c = 2 mm, and $\overline{\sigma}$ = 0.4 MPa with a misfit of 0.6 (Figures 2e and S1). The best fitting model reproduces SSEs with recurrence intervals of 2.1 years, and a duration of 16 days (Figures 2c and 2d), comparable to those observed near Gisborne. The average maximum cumulative slip of modeled SSEs (~80 mm) is smaller than that of observed SSEs (126 mm) but within the inter-SSE variability (±87 mm). The parameter space that generates reasonably small misfit is narrow (Figures 2e and S1). The simulation is very sensitive to $\overline{\sigma}$ but less so to a-b and D_c. For example, the misfit increases from 0.6 to 28.0 when $\overline{\sigma}$ increases from 0.4 to 0.5 MPa (a-b = −0.003 and Dc = 2 mm), whereas the change is less dramatic for cases with larger D_c.

3. Dynamic Perturbation

Next, we apply dynamic perturbations in the form of normal and shear stress changes resolved on the fault to the reference model (see the supporting information for details, following Wei et al., 2015, using a revised state evolution from Linker & Dieterich, 1992). Stress perturbation (period ≥3 s) is calculated in the SSE source region using a kinematic slip model of the Kaikoura mainshock (Model A in Holden et al., 2017), with the maximum amplitude uncertainty on the order of 30% (Figures S2 and S3). Due to the basin enhancing effect, the amplitude of the dynamic Coulomb stress change is comparable for depth between 5 and 16 km with larger amplitude between 8 and 12 km. (Figure S2). Another source model (Wang et al., 2018) predicts similar amplitude and duration of dynamic stress changes at these locations (Figure S4). For simplicity, we apply perturbations calculated at 12 km depth uniformly for the fault above 15 km and impose zero below 15 km. The perturbation is fine-tuned by applying constant scaling factors between 0.2 and 1.0, to account for the uncertainties in the calculation of perturbations as well as the RS model parameters.

We find that the perturbed model can reproduce the amplitude and duration of the dynamically triggered SSE in the Gisborne segment. In this scenario, the perturbation is introduced at year 14.5 (98.6% of the SSE cycle) because this segment was likely at the late stage of its ~2-year SSE cycle during the 2016 Kaikoura earthquake; the previous SSE at Gisborne occurred in September–October 2014 (Table S1). We find that the largest amplitude of the dynamic Coulomb stress change (peak $\Delta\sigma_f(t)$) mainly controls the properties of the triggered SSE, in terms of its duration and cumulative slip, and instantaneous versus delayed triggering (Figures 3a–3c). The amplitude and duration of the SSE triggered by the perturbation with a peak $\Delta\sigma_f(t)$ of 71 kPa (blue line in Figures 3a and 3b, scaling factor 0.40) are the most consistent with observation (Wallace et al., 2017). The slip history at depth is similar between the triggered and spontaneous SSE, both nucleating at about 10 km depth and simultaneously propagating upward and downward along the fault (Figure S5). A slightly smaller perturbation (red line in Figures 3a and 3b, scale factor 0.35) triggers an SSE with a delay, and a larger perturbation (magenta line in Figures 3a and 3b, scale factor 0.50) triggers a larger slip event with a shorter duration.

We also find that the displacement of instantaneously triggered SSEs increases with the peak $\Delta\sigma_f(t)$ but remains small until it reaches a threshold (~60 kPa in the case shown in Figure 3c), above which the slip increases quickly with the perturbation. For example, a perturbation with a peak $\Delta\sigma_f(t)$ of 50 kPa triggers less than 0.1 cm slip, whereas a perturbation with a peak $\Delta\sigma_f(t)$ of 71 kPa would instantaneously trigger 10 cm slip. The maximum slip velocity exceeds 1 cm/s (considered as a seismic event) when the perturbation exceeds ~85 kPa (Figure 3c). Thus, if a perturbation is sufficiently strong, the triggered slip will become seismic. However, no interplate earthquake near Gisborne was triggered by the 2016 Kaikoura earthquake. On one hand, the dynamic perturbation from the Kaikoura earthquake might not have been strong enough to trigger a large interplate earthquake. On the other hand, our fault model might miss some physics such as dilatancy strengthening (Liu & Rubin, 2010; Segall et al., 2010), which can stabilize slip so that the triggered slip remains aseismic even under very large perturbations. Besides dilatancy strengthening, the stabilizing effect can also be realized by imposing a cutoff-velocity in the RS friction model, in which a fault segment can change from VW to VS when slip velocity exceeds the preset cutoff velocity (Hawthorne & Rubin, 2013a, 2013b; Matsuzawa et al., 2013; Shibazaki et al., 2012).

To explore the effect of the timing of perturbation on triggered SSEs, we run simulations with different magnitudes of perturbations added at different times within a regular SSE cycle between years 12.44 and 14.53. We find that the timing of perturbation affects whether the next SSE is delayed, triggered with a delay, or

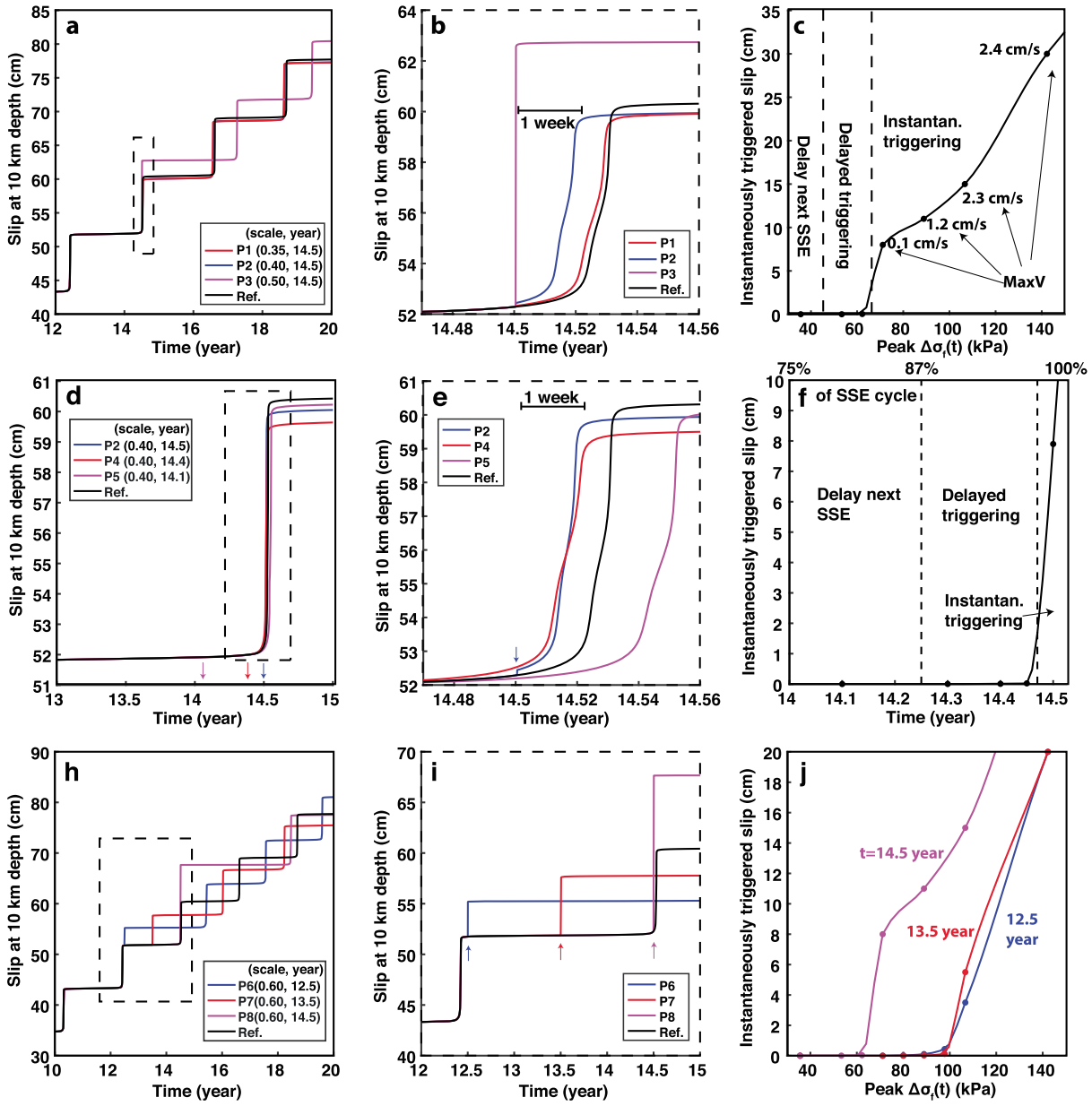

Figure 3. (a) Simulated SSEs with perturbation scaled at different levels added at the same time, 14.5 year (98.6% of the SSE cycle). The black solid line is the reference model. Perturbations are scaled at 0.35 (P1, red), 0.40 (P2, blue), and 0.50 (P3, magenta) and imposed above 12 km depth, respectively. They correspond to peak $\Delta\sigma_f(t)$ of 53, 71, and 89 kPa, respectively. The dashed box is the area shown in (b). (b) The same figure as (a) but enlarged between years 14.47 and 14.56. (c) Instantaneously triggered slip versus the peak $\Delta\sigma_f(t)$ for simulations that perturbations are added at year 14.5. The black dots are the simulation samples. The dashed line separates the cases of different effect on the next SSE. (d) Simulated SSEs with the same perturbation (scaling factor 0.40; 71 kPa) added at different times of the SSE cycle. Perturbations are added at years 14.1 (P5, magenta), 14.4 (P4, red), and 14.5 (P2, blue); 80%, 94%, and 98.6% of the SSE cycle, respectively. The dashed box is the area shown in (e). The arrows indicate the time perturbation added. (e) The same figure as (d) but enlarged between years 14.47 and 14.56. (f) Instantaneously triggered slip versus time of perturbation (and % of the SSE cycle) for simulations with peak $\Delta\sigma_f(t)$ of 71 kPa. The dots are the simulation samples. The dashed line separates the cases whether the next SSE is delayed, delayed triggered, or instantaneously triggered. (h) Simulated SSEs with the same perturbation (scaling factor 0.60; 107 kPa) added at different times of the SSE cycle. Perturbations are added at years 12.5 (P6, blue), 13.5 (P7, red), and 14.5 (P8, magenta); 3%, 50%, and 98.6% of the SSE cycle, respectively. The dashed box is the area shown in (i). (i) The same figure as (h) but enlarged between years 12 and 15. (j) Instantaneously triggered slip versus the peak $\Delta\sigma_f(t)$ for perturbations at three different times, colored the same way as (h) and (i). The dots are the simulation samples.

instantaneously triggered (Figure 3f). For the perturbation with a peak $\Delta\sigma_f(t)$ of 71 kPa, the next SSE will be delayed compared to the reference model if it is added before year 14.25 (87% of the SSE cycle). If added after year 14.25 but before 14.45 (97% of the SSE cycle), the next event will be triggered with delay. If added after year 14.45, it will be instantaneously triggered. Here we define the onset of an SSE as the slip

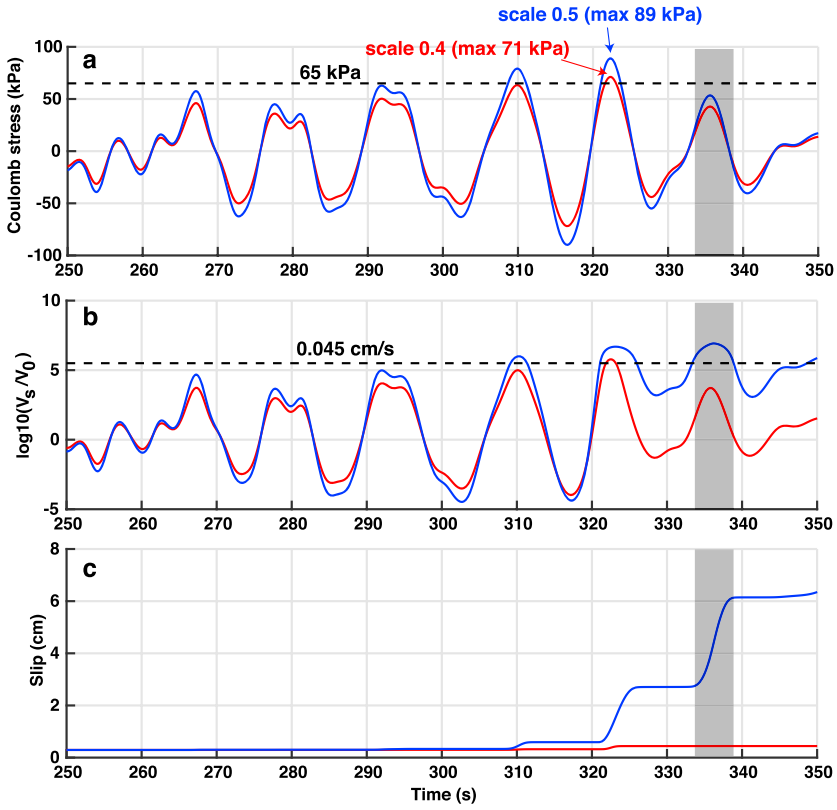

Figure 4. Effect of Coulomb stress change on the dynamic triggering of modeled SSEs during the perturbation. (a) Coulomb stress perturbations applied in cases 1 and 2. Perturbation 1 (blue solid line) is scaled to 0.5 of the simulated stress perturbation with a peak $\Delta\sigma_f(t)$ of 89 kPa. Perturbation 2 (red solid line) is scaled to 0.4 with a peak $\Delta\sigma_f(t)$ of 71 kPa. The black dashed line is the 65 kPa threshold. The gray shaded bar highlights the largest subevent. (b) Modeled fault slip velocity V_s (log scale) at 10 km depth. V_0 is the subduction rate of 45 mm/yr. The black dashed line shows a slip rate of 0.045 cm/s. (c) Modeled fault slip resulting from the two perturbations at 10 km depth.

velocity exceeds $3V_{pl}$, and the difference between delay and instantaneously triggering is whether a gap exists between the time of perturbation and SSE onset.

The trade-off effects between the magnitude and the timing of a perturbation can be further illustrated by simulation cases in Figures 3h–3j, where a sufficiently large perturbation with a peak $\Delta\sigma_f(t)$ of 107 kPa is introduced at years 12.5 (early, 3% of the SSE cycle), 13.5 (middle, 50%), and 14.5 (late, 98.6%). In all three cases detectable instantaneous slip (>1 cm) has been triggered, while the amount of triggered slip (~3.4, 5.5, and 15 cm, respectively) and the maximum slip rate increase as the perturbation is introduced later in the SSE cycle.

The triggered SSE usually consists of several individual events, each lasting less than 5 s, in phase with the imposed dynamic Coulomb stress change (blue lines in Figure 4). Noticeable slip will occur when the Coulomb stress exceeds a threshold, 65 kPa for the case shown in Figure 4. The threshold decreases after slip has accelerated following initial stress perturbations. For example, the dynamic Coulomb stress during the largest subslip event (blue line, gray shaded bar) is at 50 kPa, much smaller than the initial 65 kPa threshold. This suggests that once the perturbation amplitude exceeds an initial threshold, a longer duration of dynamic stress perturbation also promotes the dynamic triggering of the SSEs, which is consistent with proposition from Wallace et al. (2017). The exact threshold depends on the timing of perturbation, as described in the previous paragraph.

4. Conclusions and Discussion

We reproduce the timing and amplitude of spontaneous and triggered SSEs near Gisborne, New Zealand, using a RS friction model. We show that realistic perturbations estimated from a dynamic stressing model

are adequate to trigger SSEs at the timing similar to Gisborne in the SSE cycle. Low (~0.4 MPa) effective normal stress on the subduction interface is needed to reproduce the observed spontaneous SSE recurrence interval of two years and average duration of two weeks. Whether an SSE is dynamically triggered mainly depends on the timing of perturbation with respect to the SSE cycle and the maximum Coulomb stress change.

The low effective normal stress of the fault zone being dynamically triggered is consistent with lab experiment of dynamic triggering of earthquakes (Johnson et al., 2012). The stress perturbations of 65–100 kPa associated with dynamic triggering of SSEs in this study are higher than the typical range of 1–5 kPa observed in studies of the dynamic triggering of earthquakes in volcanic/geyser regions in California (Aiken & Peng, 2014; Brodsky & Prejean, 2005) and nonvolcanic tremors near Parkfield (Peng et al., 2009), but comparable to the level of transient shear stresses (40–60 kPa) triggering nonvolcanic tremors in subduction zones (Rubinstein et al., 2007) and continental thrust faults (Peng & Chao, 2008). The different threshold may be due to different background stress levels because lower triggering thresholds tend to be associated with faults in extensional or transtensional tectonic regions (Harrington & Brodsky, 2006), whereas faults with higher thresholds are mainly under compression. The different threshold may also reflect the degree to which the recipient faults are critically stressed (Figure 3), including the population of rupture sources on a particular fault and how many of them are close to failure.

Station PAWA near southern Hawkes Bay (SHB; Figure 1) started to move one week after the 2016 Kaikoura earthquake. It is possible that the SSE segment was instantaneously triggered offshore but slowly propagated landward, or that the slow slip near Gisborne triggered slip at station PAWA. Another possibility is that the segment near SHB was dynamically triggered with a one-week delay, which may be understood from our numerical simulations. Two previous SSEs have been observed in SHB in 2006 and 2011 (Wallace et al., 2017; Wallace & Beavan, 2010), suggesting that SHB is also near the end of its SSE cycle and an approximately five-year recurrence interval of SSEs in this region, which requires a larger $\overline{\sigma}$ in our fault model. Because the triggering behavior depends on the ratio of peak $\Delta\sigma_f(t)$ and $\overline{\sigma}$ in the VW zone (Figure S6), it requires a larger perturbation to instantaneously trigger SSE in SHB. As long as the timing and the ratio of peak $\Delta\sigma_f(t)$ and $\overline{\sigma}$ are within a proper range (Figure S6), the possible delayed triggering of the SSE in SHB can be explained by our model.

The upper transition from VS to VW at 5 km depth in our model is less well constrained because it is offshore. However, the amplitude of a SSE inferred from ocean bottom pressure data decreases toward the trench in this region (Wallace et al., 2016), indicating that the shallowest layer may be VS. A shallower updip end would result in a fault model with a wider SSE zone and smaller $\overline{\sigma}$ to fit the same two-year interval SSEs. In this case, a smaller peak $\Delta\sigma_f(t)$ is needed to trigger SSEs in Gisborne but the ratio of the threshold peak $\Delta\sigma_f(t)$ and $\overline{\sigma}$ remains the same (Figure S6).

To confirm that static stress had little impact on triggering SSE in our study case, we run another set of simulations using static stress perturbations at the same time of our preferred case of dynamic perturbation using the same fault model, following Liu and Rice (2007). The minimum static stress needed to instantaneously trigger a SSE of 1 cm is between 20 and 50 kPa (Figure S7), which is at least one magnitude higher than the model estimated static stress change of $<$0.7 kPa in the Gisborne SSE region due to the 2016 Kaikoura earthquake (Wallace et al., 2017). This result supports our assumption that dynamic stress perturbation is the dominant mechanism for triggering SSEs near Gisborne immediately following the 2016 Kaikoura earthquake.

Our simulation results have fundamental implications to the mechanism of SSEs. First, we demonstrate that the triggering threshold may decrease during the course of a perturbation. Once the perturbation amplitude exceeds an initial threshold, a longer duration of dynamic stress changes promotes larger slip during a dynamically triggered SSE (Figure 4). This implies that shallow SSEs are more likely to be dynamically triggered than deep SSEs because they are often located underneath a sedimentary wedge, which enhances dynamic stress changes on the plate interface (Wallace et al., 2017). This is corroborated by the very few cases of dynamically triggered deep SSEs in many subduction zones despite their close monitoring over the last ~20 years. Second, our conclusion that the triggering of SSEs depends on the timing of the SSE cycle is consistent with observations in other subduction zones (Itaba & Ando, 2011; Zigone et al., 2012). Our results suggest that instantaneous dynamic triggering of observable SSEs may be

relatively uncommon because most SSEs are probably not late in their respective SSE cycle when a large earthquake occurs nearby. Third, we show that dynamic perturbation could affect the occurrences of future SSEs even when they are relatively small and added early in the SSE cycle. This implies that some of the natural variability of the SSE interval might be influenced by dynamic perturbations. Future numerical models that simulate SSE cycles should consider incorporating dynamic perturbations from nearby or global large earthquakes.

Acknowledgments
We thank Editor Gavin Hayes and two anonymous reviewers for their constructive comments. We thank Laura Wallace for helpful discussions. M. Wei and P. Shi were supported by the National Science Foundation of United States (award 1654416). Y. Liu was supported by the Natural Science and Engineering Research Council of Canada (NSERC RGPIN 418338-12). Y. Kaneko was supported by the Rutherford Discovery Fellowship from the Royal Society of New Zealand and the New Zealand eScience Infrastructure (NeSI) high-performance computing facilities. Data from numerical modeling of this study are shown in the main text; GPS data used in Figure can be obtained at www.geonet.org.nz.

References

Aiken, C., & Peng, Z. (2014). Dynamic triggering of microearthquakes in three geothermal/volcanic regions of California. *Journal of Geophysical Research: Solid Earth*, *119*, 6992–7009. https://doi.org/10.1002/2014JB011218

Araki, E., Saffer, D. M., Kopf, A. J., Wallace, L. M., Kimura, T., Machida, Y., & Ide, S. (2017). Recurring and triggered slow slip events near the trench at the Nankai Trough subduction megathrust. *Science*, *356*(6343), 1157–1160. https://doi.org/10.1126/science.aan3120

Audet, P., Bostock, M. G., Christensen, N. I., & Peacock, S. M. (2009). Seismic evidence for overpressured subducted oceanic crust and megathrust fault sealing. *Nature*, *457*(7225), 76–78. https://doi.org/10.1038/nature07650

Brodsky, E., & Prejean, S. G. (2005). New constraints on mechanisms of remotely triggered seismicity at Long Valley Caldera. *Journal of Geophysical Research*, *110*, B04302. https://doi.org/10.1029/2004JB003211

Dragert, G., Wang, K., & James, T. S. (2001). A silent slip event on the deeper Cascadia subduction interface. *Science*, *292*(5521), 1525–1528. https://doi.org/10.1126/science.1060152

Eberhart-Phillips, D., & Bannister, S. (2015). 3-D imaging of the northern Hikurangi subduction zone, New Zealand: Variations in subducted sediment, slab fluids and slow slip. *Geophysical Journal International*, *201*(2), 838–855. https://doi.org/10.1093/gji/ggv057

Gomberg, J., Beeler, N., & Blanpied, M. (1998). Earthquake triggering by transient and static deformations. *Journal of Geophysical Research*, *103*(B10), 24,411–24,426. https://doi.org/10.1029/98JB01125

Harrington, R. M., & Brodsky, E. E. (2006). The absence of remotely triggered seismicity in Japan. *Bulletin of the Seismological Society of America*, *96*(3), 871–878. https://doi.org/10.1785/0120050076

Hawthorne, J. C., & Rubin, A. M. (2013a). Laterally propagating slow slip events in a rate and state friction model with a velocity-weakening to velocity-strengthening transition. *Journal of Geophysical Research: Solid Earth*, *118*, 3785–3808. https://doi.org/10.1002/jgrb.50261

Hawthorne, J. C., & Rubin, a. M. (2013b). Tidal modulation and back-propagating fronts in slow slip events simulated with a velocity-weakening to velocity-strengthening friction law. *Journal of Geophysical Research: Solid Earth*, *118*, 1216–1239. https://doi.org/10.1002/jgrb.50107

Holden, C., Kaneko, Y., D'Anastasio, E., Benites, R., Fry, B., & Hamling, I. J. (2017). The 2016 Kaikoura earthquake revealed by kinematic source inversion and seismic wavefield simulations: Slow rupture propagation on a geometrically complex crustal fault network. *Geophysical Research Letters*, *44*, 11,320–11,328. https://doi.org/10.1002/2017GL075301

Itaba, S., & Ando, R. (2011). A slow slip event triggered by teleseismic surface waves. *Geophysical Research Letters*, *38*, L21306. https://doi.org/10.1029/2011GL049593

Johnson, P. A., Carpenter, B., Knuth, M., Kaproth, B. M., Le Bas, P.-Y., Daub, E. G., & Marone, C. (2012). Nonlinear dynamical triggering of slow slip on simulated earthquake faults with implications to Earth. *Journal of Geophysical Research*, *117*, B04310. https://doi.org/10.1029/2011JB008594

Kaneko, Y., & Lapusta, N. (2008). Variability of earthquake nucleation in continuum models of rate-and-state faults and implications for aftershock rates. *Journal of Geophysical Research*, *113*, B12312. https://doi.org/10.1029/2007JB005154

Lapusta, N., Rice, J. R., Ben-Zion, Y., & Zheng, G. (2000). Elastodynamic analysis for slow tectonic loading with spontaneous rupture episodes on faults with rate- and state-dependent friction. *Journal of Geophysical Research*, *105*(B10), 23,765–23,789. https://doi.org/10.1029/2000JB900250

Li, D., & Liu, Y. (2016). Spatiotemporal evolution of slow slip events in a nonplanar fault model for northern Cascadia subduction zone. *Journal of Geophysical Research: Solid Earth*, *121*, 6828–6845. https://doi.org/10.1002/2016JB012857

Li, D., & Liu, Y. (2017). Modeling slow-slip segmentation in Cascadia subduction zone constrained by tremor locations and gravity anomalies. *Journal of Geophysical Research: Solid Earth*, *122*, 3138–3157. https://doi.org/10.1002/2016JB013778

Li, H., Wei, M., Li, D., Liu, Y., Kim, Y., & Zhou, S. (2018). Segmentation of slow slip events in South Central Alaska possibly controlled by a subducted oceanic plateau. *Journal of Geophysical Research: Solid Earth*, *123*, 418–436. https://doi.org/10.1002/2017JB014911

Linker, M., & Dieterich, J. (1992). Effects of variable normal stress on rock friction: Observations and constitutive equations. *Journal of Geophysical Research*, *97*(B4), 4923–4940. https://doi.org/10.1029/92JB00017

Liu, Y., & Rice, J. R. (2007). Spontaneous and triggered aseismic deformation transients in a subduction fault model. *Journal of Geophysical Research*, *112*, B09404. https://doi.org/10.1029/2007JB004930

Liu, Y., & Rubin, A. M. (2010). Role of fault gouge dilatancy on aseismic deformation transients. *Journal of Geophysical Research*, *115*, B10414. https://doi.org/10.1029/2010JB007522

Luo, Y. (2018). Earthquake moment-area scaling relations and the effect of fault heterogeneity on slow to fast earthquake slip. Dissertation (Ph.D.), California Institute of Technology. https://doi.org/10.7907/Z9SQ8XMV

Luo, Y., & Ampuero, J. P. (2017). Stability of faults with heterogeneous friction properties and effective normal stress. *Tectonophysics*, *733*, 257–272. https://doi.org/10.1016/j.tecto.2017.11.006

Matsuzawa, T., Shibazaki, B., Obara, K., & Hirose, H. (2013). Comprehensive model of short- and long-term slow slip events in the Shikoku region of Japan, incorporating a realistic plate configuration. *Geophysical Research Letters*, *40*, 5125–5130. https://doi.org/10.1002/grl.51006

Miyazawa, M., & Brodsky, E. E. (2008). Deep low-frequency tremor that correlates with passing surface waves. *Journal of Geophysical Research*, *113*, B01307. https://doi.org/10.1029/2006JB004890

Peng, Z., & Chao, K. (2008). Non-volcanic tremor beneath the Central Range in Taiwan triggered by the 2001 M_w 7.8 Kunlun earthquake. *Geophysical Journal International*, *175*(2), 825–829. https://doi.org/10.1111/j.1365-246X.2008.03886.x

Peng, Z., & Gomberg, J. (2010). An integrated perspective of the continuum between earthquakes and slow-slip phenomena. *Nature Geoscience*, *3*(9), 599–607. https://doi.org/10.1038/ngeo940

Peng, Z., Vidale, J. E., Wech, A. G., Nadeau, R. M., & Creager, K. C. (2009). Remote triggering of tremor along the San Andreas Fault in central California. *Journal of Geophysical Research*, *114*, B00A06. https://doi.org/10.1029/2008JB006049

Perfettini, H., Schmittbuhl, J., & Cochard, A. (2003a). Shear and normal load perturbations on a two-dimensional continuous fault: 1. Static triggering. *Journal of Geophysical Research*, *108*(B9), 2408. https://doi.org/10.1029/2002JB001804

Perfettini, H., Schmittbuhl, J., & Cochard, A. (2003b). Shear and normal load perturbations on a two-dimensional continuous fault: 2. Dynamic triggering. *Journal of Geophysical Research*, *108*(B9), 2409. https://doi.org/10.1029/2002JB001805

Rogers, G., & Dragert, H. (2003). Episodic tremor and slip on the Cascadia subduction zone: The chatter of silent slip. *Science*, *300*(5627), 1942–1943. https://doi.org/10.1126/science.1084783

Rubin, A. M. (2008). Episodic slow slip events and rate-and-state friction. *Journal of Geophysical Research*, *113*, B11414. https://doi.org/10.1029/2008JB005642

Rubinstein, J. L., Vidale, J. E., Gomberg, J., Bodin, P., Creager, K. C., & Malone, S. D. (2007). Non-volcanic tremor driven by large transient shear stresses. *Nature*, *448*(7153), 579–582. https://doi.org/10.1038/nature06017

Saffer, D. M., & Wallace, L. M. (2015). The frictional, hydrologic, metamorphic and thermal habitat of shallow slow earthquakes. *Nature Geoscience*, *8*(8), 594–600. https://doi.org/10.1038/ngeo2490

Schwartz, S. Y., & Rokosky, J. M. (2007). Slow slip events and seismic tremor at circum-Pacific subduction zones. *Reviews of Geophysics*, *45*, RG3004. https://doi.org/10.1029/2006RG000208

Segall, P., Rubin, A. M., Bradley, A. M., & Rice, J. R. (2010). Dilatant strengthening as a mechanism for slow slip events. *Journal of Geophysical Research*, *115*, B12305. https://doi.org/10.1029/2010JB007449

Shelly, D. R., Beroza, G. C., Ide, S., & Nakamula, S. (2006). Low-frequency earthquakes in Shikoku, Japan, and their relationship to episodic tremor and slip. *Nature*, *442*(7099), 188–191. https://doi.org/10.1038/nature04931

Shibazaki, B., Obara, K., Matsuzawa, T., & Hirose, H. (2012). Modeling of slow slip events along the deep subduction zone in the Kii Peninsula and Tokai regions, southwest Japan. *Journal of Geophysical Research*, *117*, B06311. https://doi.org/10.1029/2011JB009083

Wallace, L. M., & Beavan, J. (2010). Diverse slow slip behavior at the Hikurangi subduction margin, New Zealand. *Journal of Geophysical Research*, *115*, B12402. https://doi.org/10.1029/2010JB007717

Wallace, L. M., Beavan, J., Bannister, S., & Williams, C. (2012). Simultaneous long-term and short-term slow slip events at the Hikurangi subduction margin, New Zealand: Implications for processes that control slow slip event occurrence, duration, and migration. *Journal of Geophysical Research*, *117*, B11402. https://doi.org/10.1029/2012JB009489

Wallace, L. M., Beavan, J., McCaffrey, R., & Darby, D. (2004). Subduction zone coupling and tectonic block rotations in the North Island, New Zealand. *Journal of Geophysical Research*, *109*, B12406. https://doi.org/10.1029/2004JB003241

Wallace, L. M., & Eberhart-Phillips, D. (2013). Newly observed, deep slow slip events at the central Hikurangi margin, New Zealand: Implications for downdip variability of slow slip and tremor, and relationship to seismic structure. *Geophysical Research Letters*, *40*, 5393–5398. https://doi.org/10.1002/2013GL057682

Wallace, L. M., Hreinsdottir, S., Ellis, S., Hamling, I., D'Anastasio, E., & Denys, P. (2018). Triggered slow slip and afterslip on the southern Hikurangi subduction zone following the Kaikōura earthquake. *Geophysical Research Letters*, *45*. http://doi.org/10.1002/2018GL077385

Wallace, L. M., Kaneko, Y., Hreinsdóttir, S., Hamling, I., Peng, Z., Bartlow, N., et al. (2017). Large-scale dynamic triggering of shallow slow slip enhanced by overlying sedimentary wedge. *Nature Geoscience*, *10*(10), 765–770. https://doi.org/10.1038/ngeo3021

Wallace, L. M., Webb, S. C., Ito, Y., Mochizuki, K., Hino, R., Henrys, S., et al. (2016). Slow slip near the trench at the Hikurangi subduction zone, New Zealand. *Science*, *352*(6286), 701–704. https://doi.org/10.1126/science.aaf2349

Wang, T., Wei, S., Shi, X., Qiu, Q., Li, L., Peng, D., et al. (2018). The 2016 Kaikōura earthquake: Simultaneous rupture of the subduction interface and overlying faults. *Earth and Planetary Science Letters*, *482*, 44–51. https://doi.org/10.1016/j.epsl.2017.10.056

Watkins, W. D., Colella, H. V., Brudzinski, M. R., Richards-dinger, K. B., & Dieterich, J. H. (2015). The role of effective normal stress, frictional properties, and convergence rates in characteristics of simulated slow slip events. *Geophysical Research Letters*, *42*, 1061–1067. https://doi.org/10.1002/2014GL062794

Wei, M., Kaneko, Y., Liu, Y., & McGuire, J. J. (2013). Episodic fault creep events in California controlled by shallow frictional heterogeneity. *Nature Geoscience*, *6*(7), 566–570. https://doi.org/10.1038/ngeo1835

Wei, M., Liu, Y., Kaneko, Y., McGuire, J. J., & Bilham, R. (2015). Dynamic triggering of creep events in the Salton Trough, Southern California by regional M ≥5.4 earthquakes constrained by geodetic observations and numerical simulations. *Earth and Planetary Science Letters*, *427*, 1–10. https://doi.org/10.1016/j.epsl.2015.06.044

Williams, C. A., Eberhart-Phillips, D., Bannister, S. C., Barker, D. H. N., Henrys, S., Reyners, M., & Sutherland, R. (2013). Revised interface geometry for the Hikurangi subduction zone, New Zealand. *Seismological Research Letters*, *84*(6), 1066–1073. https://doi.org/10.1785/0220130035

Zigone, D., Rivet, D., Radiguet, M., Campillo, M., Voisin, C., Cotte, N., et al. (2012). Triggering of tremors and slow slip event in Guerrero, Mexico, by the 2010 Mw 8.8 Maule, Chile, earthquake. *Journal of Geophysical Research*, *117*, B09304. https://doi.org/10.1029/2012JB009160

Geophysical Research Letters

Supporting Information for

Numerical modeling of dynamically triggered shallow slow slip events in New Zealand by the 2016 M_w 7.8 Kaikoura earthquake

Meng Wei[1], Yoshihiro Kaneko[2], Pengcheng Shi[1], Yajing Liu[3]

[1]University of Rhode Island, United States. [2]GNS Science, New Zealand. [3]McGill University, Canada.

Contents of this file

- Table S1
- Figures S1 to S7
- Basic equations and parameter setting of the basic rate-and-state code
- Implementing dynamic perturbation to the rate-and-state friction code

Table S1. List of shallow SSEs near Gisborne, Northern Hikurangi

Start time (decimal years)	Interval (decimal years)	Duration (days)	Depth (km)	Max slip depth (km)	Max slip (mm)	Mw	References
2004.875		17	<15	12	180	6.7	Wallace & Beavan, 2010
2006.521	1.646	6	<15	12	40	6.6	Wallace & Beavan, 2010
2008.210*	1.689	15	<15	13	85	6.7	Wallace & Beavan, 2010
2010.211	2.236	16	<15	13	125	6.7	Wallace & Beavan, 2010
2011.948	1.737	11	<15	12	55	6.5	Wallace et al., 2012
2014.740	2.792	24	<12	7	270	6.8	Personal communications (L. Wallace)
Average	2.0±0.5	15±6			126±87		
2016.872	2.132	7	<12	7.5	65	6.8	Wallace et al., 2017a (Dynamically triggered)

* This SSE centered slightly south of Gisborne but ruptured the center of Gisborne segment.

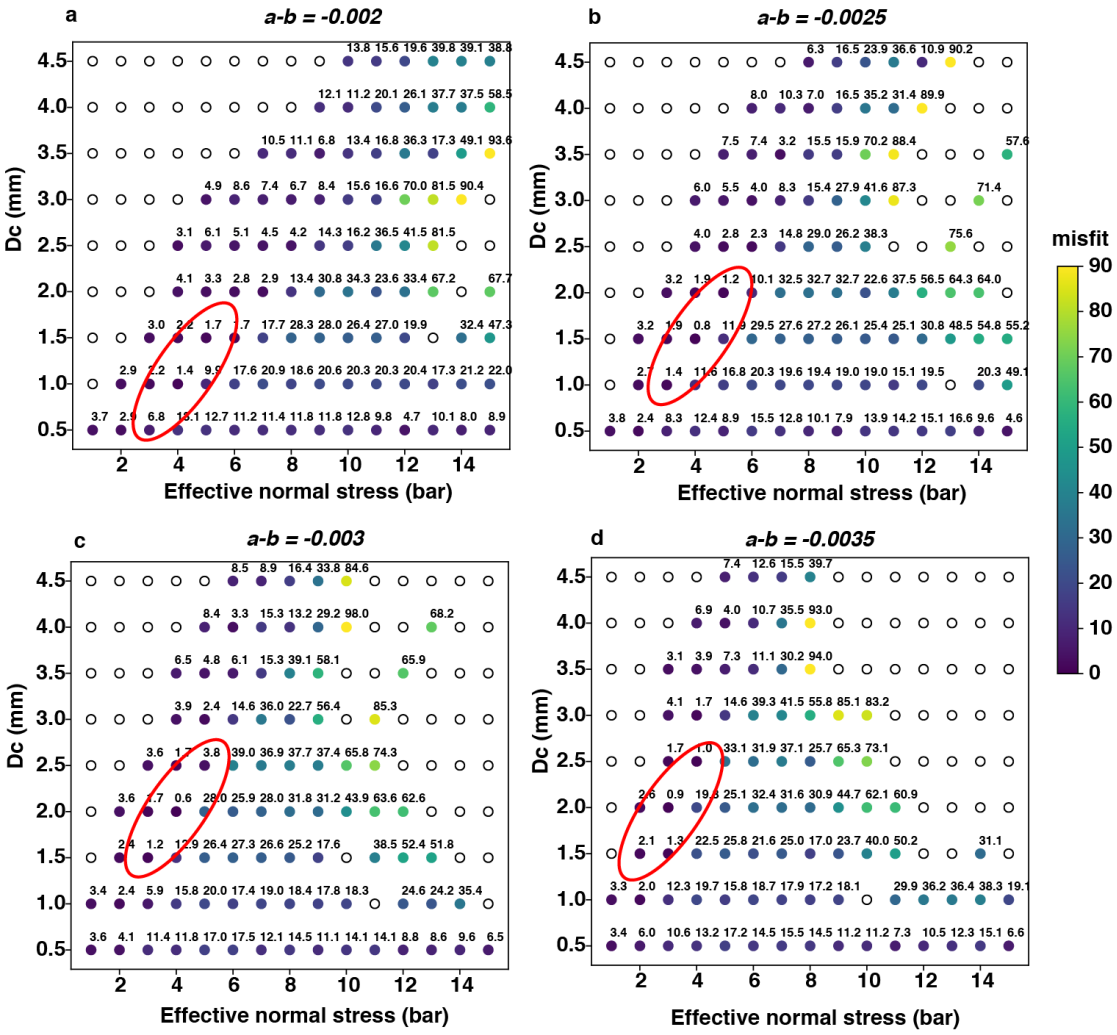

Figure S1. Phase diagram illustrating the dependence of the SSE behavior on input friction parameters. (a-d) misfit of grid search for a-b = -0.002, -0.0025, -0.003, and -0.0035, respectively. The numbers near the circles show the misfit for that simulation. The red ellipses highlight the minimum misfit. We searched the grid between 1-15 bar $\bar{\sigma}$, and 0.5-4.5 mm Dc. The open circles are cases where no repeating SSEs occur between year 10-20 years in the simulation. The red ellipses show the region near the minimum misfit in the sub-figure. The model with the minimum misfit is a-b = -0.003, $\bar{\sigma}$ = 0.4 MPa, Dc = 2 mm, and a misfit of 0.6. Note that a full range of input parameters is not explored in this study. However, the SSE behavior can be summarized by the ratio of the nucleation size and the width of the VW zone, as shown in Wei et al. (2013).

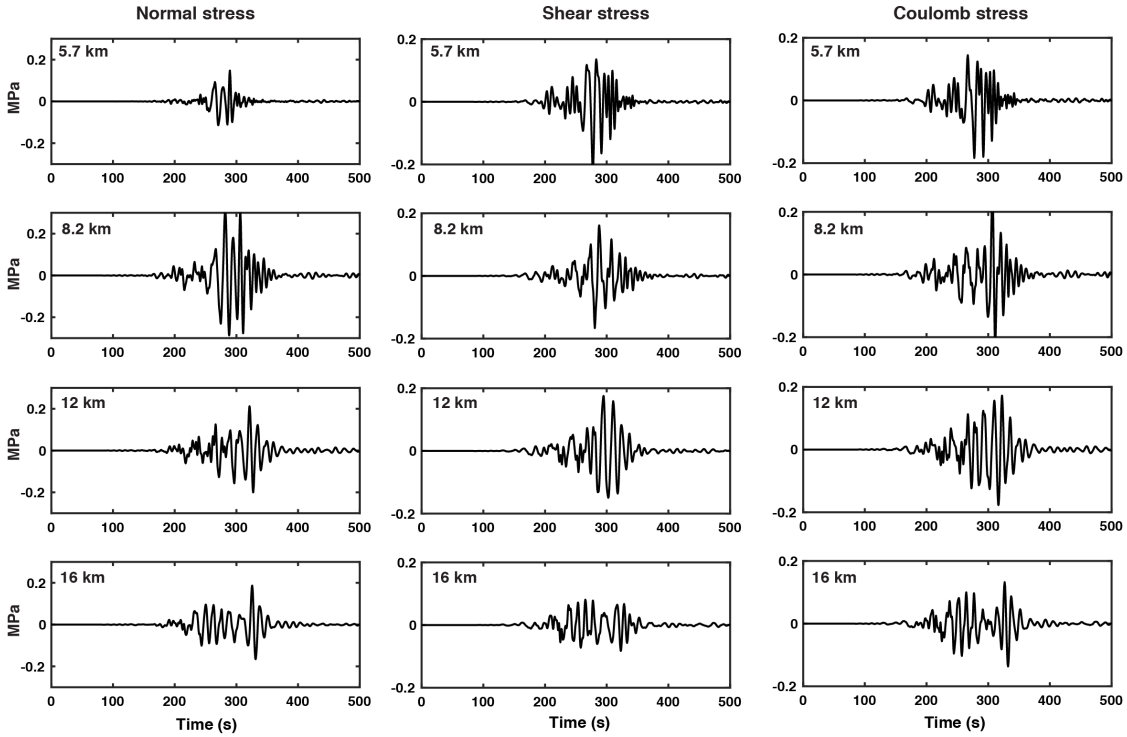

Figure S2. Dynamic perturbations on the subduction interface at different depth near Gisborne, Northern Hikurangi (Holden et al., 2017). From left to right, shear, normal, and Coulomb stress, positive promotes slip. The friction coefficient is set to 0.6 when calculating the Coulomb stress.

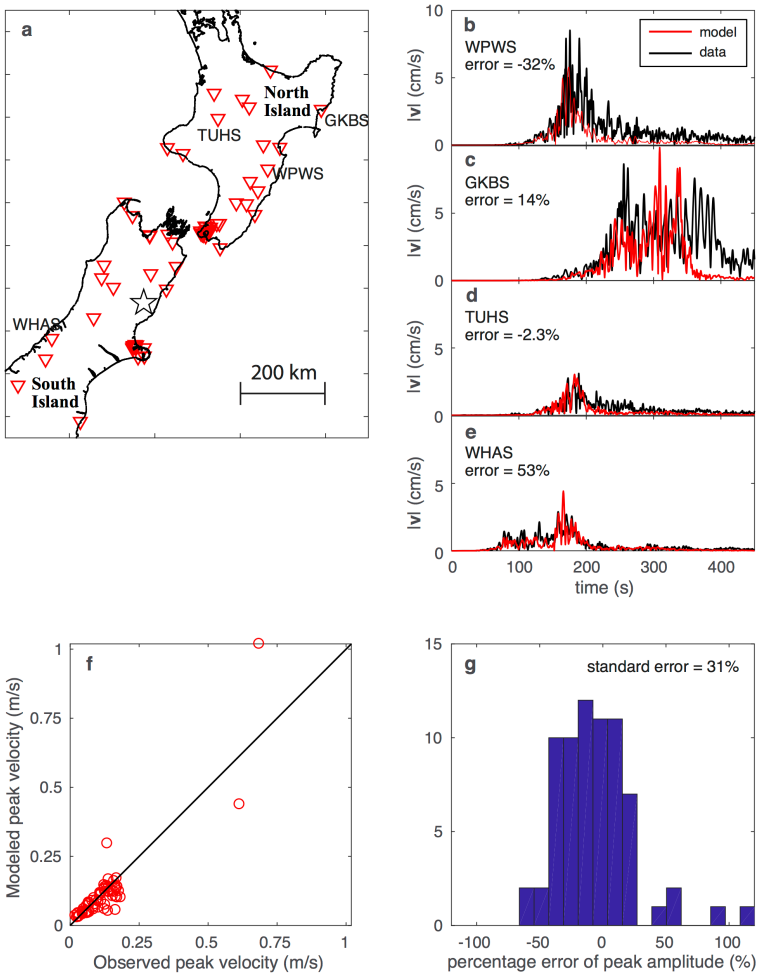

Figure S3. Assessment of the accuracy of dynamic stress changes, which are approximately proportional to the amplitude of velocity seismograms. The assumed source model is from Holden et al. (2017) which includes relatively small moment release (~8% of the total) from the Hikurangi subduction interface. (a) A map of strong-motion stations (inverted triangles) used to compare observed and computed velocity waveforms. More than 80% of the stations shown here were not used during the development of the source model described in Holden et al. (2017). Star shows the epicenter of the Kaikoura earthquake. (b – e) Observed (black) and modeled (red) magnitude of three-component velocity waveforms |v| at selected stations. Waveforms recorded in the east coast of the North Island show amplified and long-lasting ground motions due to the off-shore, low-velocity wedge. (g) Comparison of observed and modeled maximum |v| at all the stations shown in the map. (f) Histograms of percentage errors of the maximum |v| between observed and modeled waveforms: error = $(\max(|v|_{model}) - \max(|v|_{data}))/ \max(|v|_{data})$. The indicated standard error in the maximum |v| is likely comparable, or a similar order to that of the maximum dynamic stress changes.

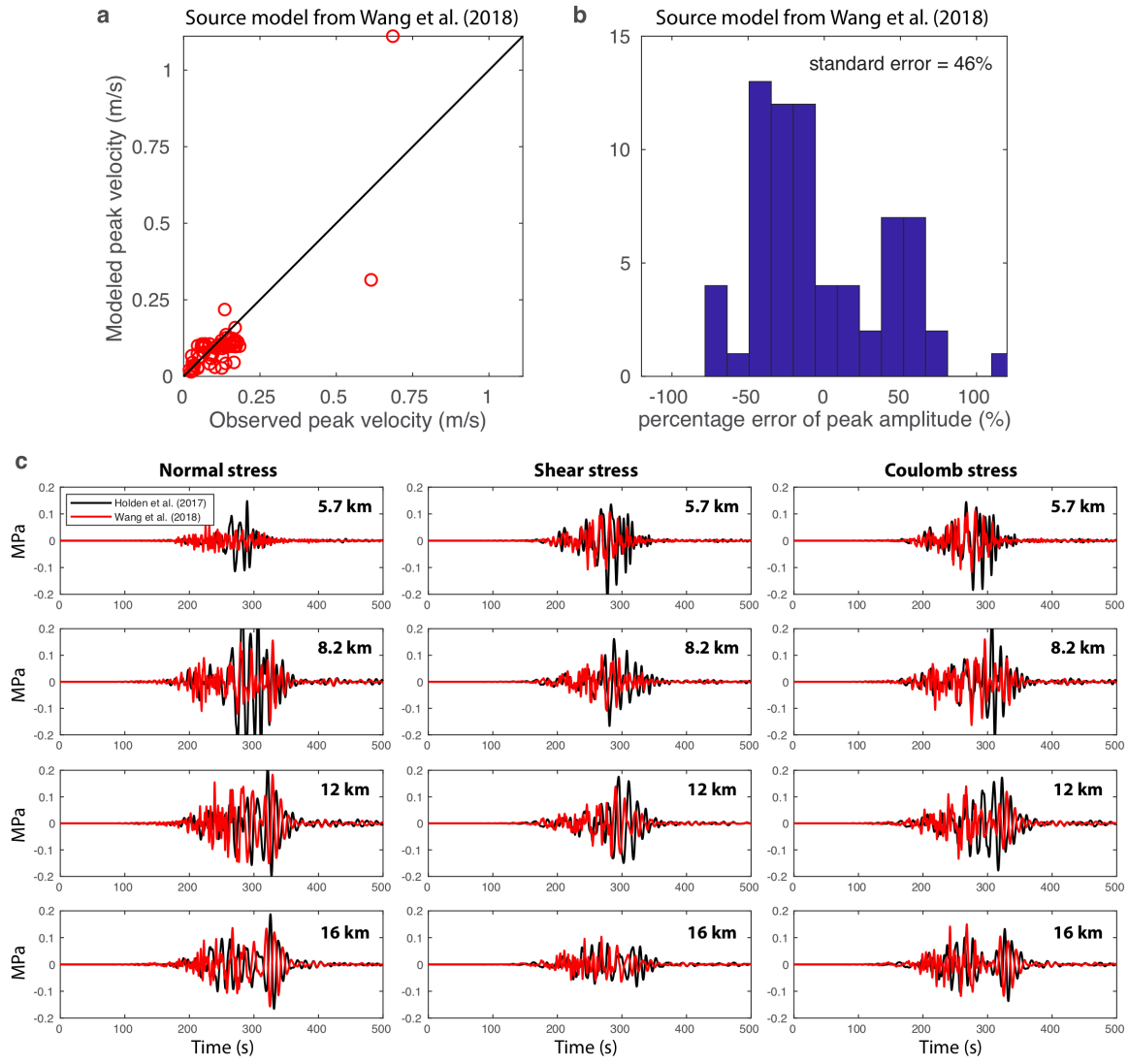

Figure S4. Sensitivity of dynamic stress changes to different assumed source models. (a) Comparison of observed and modeled maximum |v| at all the stations shown in Figure S3(a) using the source model from Wang et al. (2018), which includes large moment release (~45% of the total) from the Hikurangi subduction interface. (b) Histograms of percentage errors of the maximum |v| between observed and modeled waveforms: error = $(\max(|v|_{model}) - \max(|v|_{data}))/\max(|v|_{data})$. Compared to Holden et al.'s source model, Wang et al.'s model yields slightly larger misfits. (c) Dynamic perturbations on the subduction inferface at different depths near Gisborne derived from two different source models. The friction coefficient is set to 0.6 when calculating the Coulomb stress. Both the amplitudes and durations of dynamic stress changes for these source models are comparable.

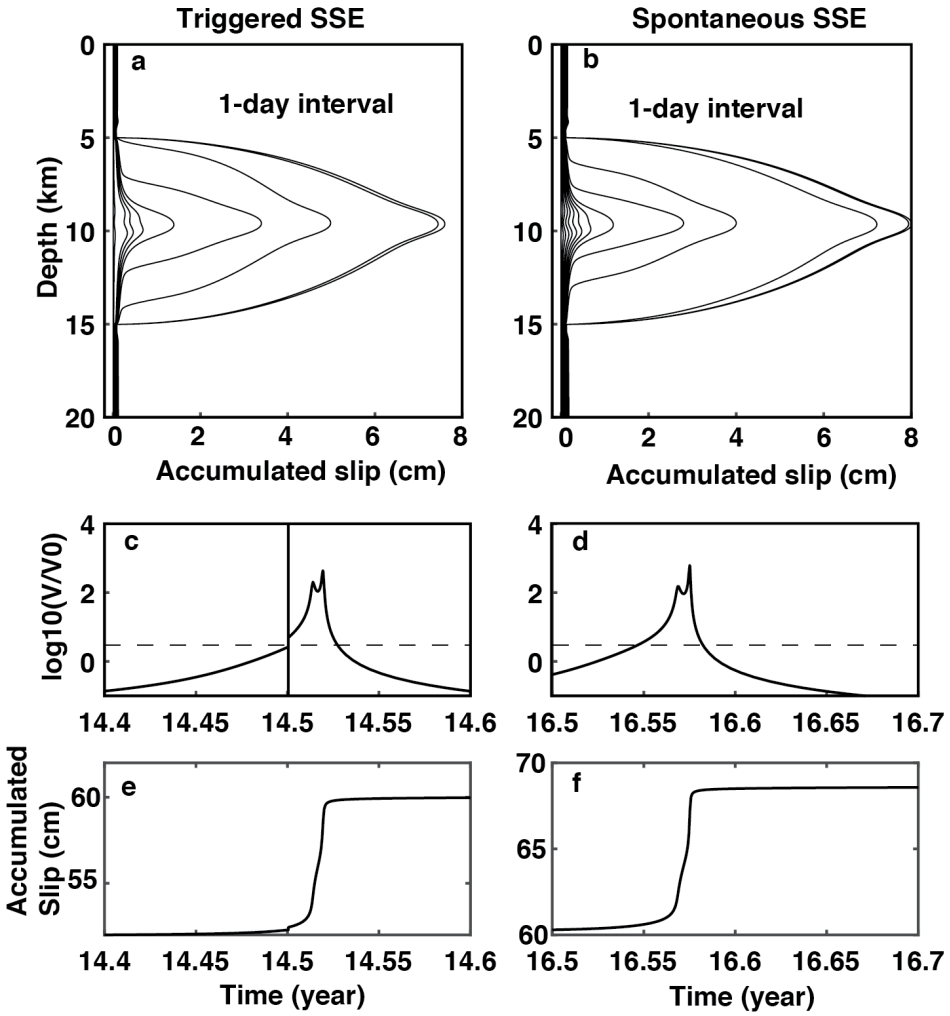

Figure S5. Simulation results of a triggered SSE and a spontaneous SSE. Parameter setting is the same as the blue line in Figure 3b, perturbation added at year 14.5 with a peak $\Delta\sigma_f(t)$ of 71 kPa. (a, b) Slip history of the triggered SSE and the spontaneous SSE, respectively. The solid lines denote slip accumulation every day. (c, d) Slip velocity at 10 km depth for the triggered and spontaneous SSE. The dashed line shows the threshold of SSE onset. (e, f) Accumulated slip at 10 km depth for the triggered and spontaneous SSE.

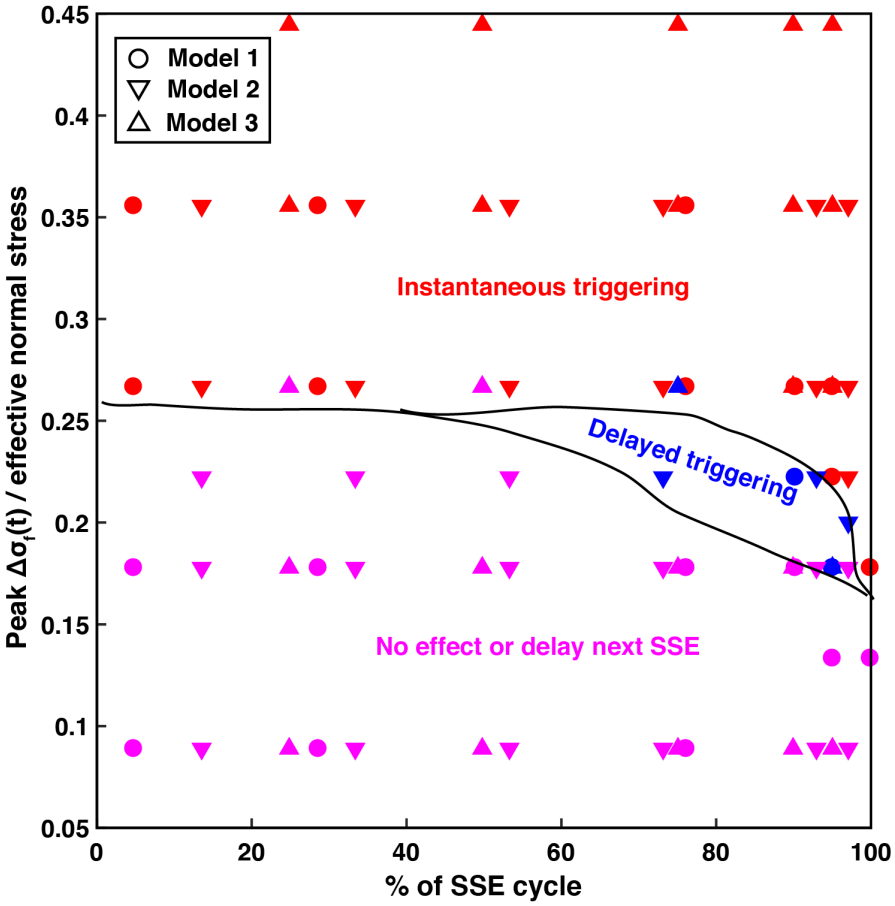

Figure S6. Phase diagram for three sets of models. Model 1: 2-year interval SSEs between 5-15 km depth ($\bar{\sigma}$ = 0.4 MPa, *Dc* = 2 mm in VW zone). Model 2: 5-year interval SSEs between 5-15 km depth ($\bar{\sigma}$ = 1.0 MPa, *Dc* = 5 mm in VW zone). Model 3: 2-year interval SSEs between 1-15 km depth ($\bar{\sigma}$ = 0.2 MPa, *Dc* = 2 mm in VW zone). The magenta, blue, and red color shows cases with no triggering, delayed triggering, and instantaneously triggering, respectively. Note that the triggering threshold is proportional to the $\bar{\sigma}$ in the VW zone in the model.

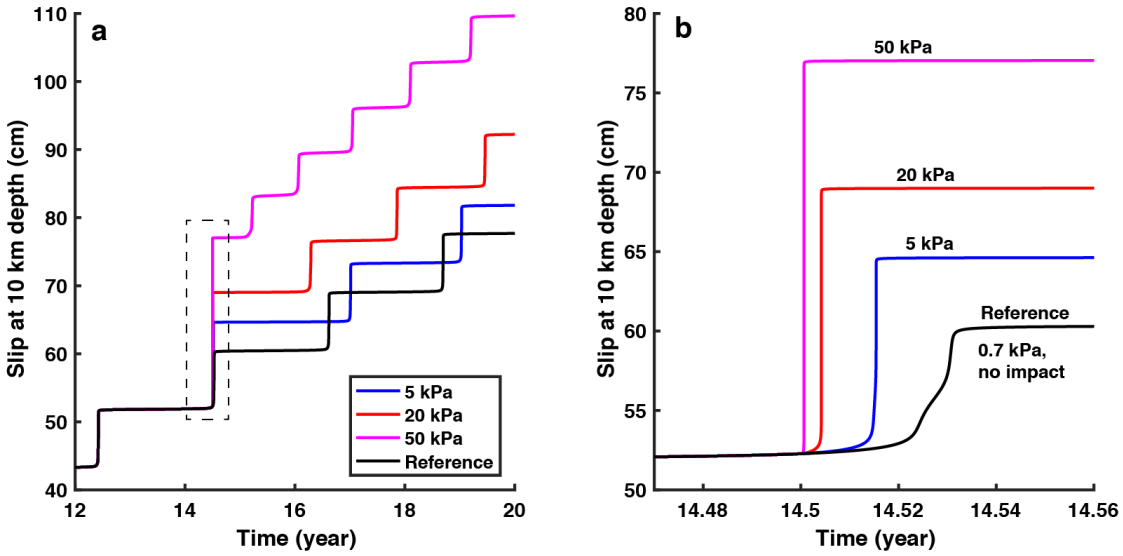

Figure S7. (a) Simulated SSEs with static stress perturbations. The black solid line is the reference model. The blue, red, magenta lines show simulations with a reduction of $\bar{\sigma}$ of 5, 20, and 50 kPa, respectively, at year 14.5, all promoting fault slip. The dashed box is the area shown in (b). (b) The same figure as (a) but enlarged between year 14.47 and 14.56. A static stress change of <0.7 kPa, estimated in the Gisborne SSE region due to the 2016 Kaikoura earthquake (Wallace et al. 2017a), has no impact on the SSE cycles in our simulations, further supporting the dynamic triggering of the SSE.

Basic equations and parameter setting of the basic rate-state code

In the RS framework, the shear stress τ evolves with slip rate V and slip history (state variable θ) as: $\tau = \bar{\sigma} f = \bar{\sigma}\left[f_0 + a\ln\left(\frac{V}{V_0}\right) + b\ln\left(\frac{V_0\theta}{D_c}\right)\right]$, where $\bar{\sigma}$ is the effective normal stress (applied normal stress minus pore pressure), D_c is the critical slip distance (the sliding distance required to renew the contact population on the sliding surface following a velocity step), *a, b* are friction parameters, and f_0 (=0.6) is the friction coefficient at a reference velocity V_0 (=1 μm/s) at steady state. We adopt the aging law $\frac{d\theta}{dt} = 1 - \frac{V\theta}{D_c}$ for the evolution of the state variable.

Implimenting dynamic perturbation to the rate-state friction code

According to Linker & Dieterich (1992), the state evolution law becomes

$$\frac{d\theta}{dt} = 1 - \frac{V\theta}{D_c} - \alpha\frac{\theta}{b\bar{\sigma}}\frac{d\bar{\sigma}}{dt} \qquad (1)$$

when effective normal stress is variable with time. Conceptually, an increase in normal stress introduces a new population of asperity contacts of younger ages than that is already present before the extra loading, and therefore the average age (state) of the new group of contacts decreases.

The following is involved for introducing dynamic perturbations. Equating shear stress from elasticity (quasi-dynamic) to that defined by rate-state friction:

$$\tau = \sigma\left[f_0 + a\ln\left(\frac{V}{V_0}\right) + b\ln\left(\frac{V_0\theta}{D_c}\right)\right] = \tau_0 - \sum K_{ij}\left(\delta_j - V_{pl}t\right) - \eta V\,, \qquad (2)$$

where τ_0 is the background shear stress. Take time derivatives of the above equation and re-organize, we get

$$\frac{dV}{dt} = \frac{-1}{a\bar{\sigma}/V + \eta}\left[\sum K_{ij}\left(\delta_j - V_{pl}\right) + \frac{b\bar{\sigma}}{\theta}\frac{d\theta}{dt} + f\frac{d\bar{\sigma}}{dt} - \frac{d\tau_0}{dt}\right] \qquad (3)$$

where friction coefficient $f = f_0 + a\ln(V/V_0) + b\ln(V_0\theta/D_c)$. Therefore, we can solve the coupled Equation (1) and (3) for dynamic perturbations. Note that $d\bar{\sigma}/dt$, $d\tau_0/dt$ and $\bar{\sigma}$ are also time-variables.